Synthesis, microstructure and mechanical properties of W-S-C self-lubricant thin films deposited by magnetron sputtering

Todor Vuchkov [ab*], Manuel Evaristo [b], Talha bin Yaqub [ab], Tomas Polcar [cd], Albano Cavaleiro[ab]

[a] IPN - LED & MAT - Instituto Pedro Nunes, Laboratory for Wear, Testing and Materials, Rua Pedro Nunes, Coimbra, Portugal

[b] SEG-CEMMPRE, Department of Mechanical Engineering, University of Coimbra, Rua Luís Reis Santos, 3030-788 Coimbra, Portugal

[c] Department of Control Engineering, Faculty of Electrical Engineering, Czech Technical University in Prague, Technická 2, Prague 6, Czech Republic

[d] nCATS, University of Southampton, University Road, Southampton SO17 1BJ, UK

* Corresponding author: Tel. +351239700900 E-mail address: todor.vuchkov@ipn.pt

Abstract

W-S-C thin films were deposited by magnetron sputtering in a semi-industrial deposition unit. Various parameters like the composition, crystallinity, morphology and hardness were studied. A single coating was selected for tribological studies in different testing environments. The tribological response during ambient air testing was governed mainly by carbon-based phase at low normal loads and both carbon-based and WS_2 rich tribofilms at higher loads. Very low coefficients of friction (~0.01) were obtained during testing at elevated temperature due to accelerated formation of WS_2 rich tribofilms. The tribological response in a vacuum against a steel-based counterbody was unsatisfactory due to the presence of a carbon-phase at the sliding interface. Discrepancies were observed between the tribological response in dry N_2 and vacuum environments.

Keywords: Magnetron sputtering; Transition-metal dichalcogenides; Self-lubricant; Tribology

1. Introduction

Transition metal dichalcogenides (TMD) are compounds consisting of a transition metal (Mo, W, Nb) and a chalcogen atom (S,Se,Te). Due to their unique lubricious properties, their usage

as thin-film coatings for mechanical components was pursued in the last 40-50 years starting with the early experiment done by Spalvins [1]. The lubricity of TMD materials is a result of their microstructure; they are crystallizing in a hexagonal structure consisting of sheets of transition metal layer sandwiched between layers made of chalcogen atoms, with the bonding within the "sandwich" being of covalent type. The bonding between the "sandwiches" is of van der Waals type resulting in interplanar mechanical weakness, which, under shear forces, promotes an easy intracrystalline slip, thus, providing lubrication [2].

The biggest disadvantage of pure sputtered TMDs is their low load-bearing capacity since they have low hardness. Depending on the morphology, deposition conditions and stoichiometry, their hardness can vary between 0.3-2 GPa. Pure TMD coatings deposited by sputtering techniques, with the ratio between the chalcogen atoms and transition metal atoms being higher than 1.5, often have a columnar structure which is porous by nature and sensitive to environmental attacks, resulting in unsatisfactory behavior during tribological testing in humid environments [3–7]. Based on their intrinsic properties, the early applications for these materials were intended mainly for space applications [8]. Many attempts were performed to make TMD materials (mainly synthesized as thin films) viable for applications involving sliding in humid environments, especially by doping them with metals [9], carbon [10–13] and nitrogen [14].

Titanium doping of sputtered MoS_2 coatings was performed by Teer et al. [9,15,16]. The authors reported a low coefficient of friction during dry sliding in a normal atmosphere with values of ~0.06-0.08. Very good performance was also observed during sliding under dry N_2 against steel counterbody with wear life of 1,900,000 cycles. In a more recent study [17], tribological testing was performed on pure and Ti doped MoS_2 coatings in ultra-high vacuum environments against steel counterbody. The authors observed an increasing friction coefficient

of the Ti-doped coating (up to 0.5) while the pure MoS_2 coating showed a much lower and stable coefficient of friction of ~0.05.

Titanium addition was also performed for sputtered WS_2 coatings by Scharf et al [3]. Co-sputtering of Ti resulted in a more amorphous structure, with the presence of nanocrystalline WS_2 and overall densification of the coating. The denser microstructures provided better tribological performance during testing at room temperature and at elevated temperatures.

Co-deposition of carbon and WS_2 performed by Voevodin et al. [10] resulted in a nanocomposite structure consisting of WS_2, amorphous carbon (a-C) and tungsten carbide (WC) phases providing "adaptive" tribological responses while sliding in diverse environments: the a-C phase was governing the friction when sliding in humid air whereas the TMD phase provided low friction while sliding in dry nitrogen and high vacuum. Further studies performed by Polcar et al. [11,13,18] have shown that nanocomposite TMD-C thin films, mainly deposited by radio frequency (RF) magnetron sputtering have non-Amonton tribological response with lower friction coefficient with increasing normal loads, inversely to what was shown before, these authors proved that the TMD phase was also governing the friction during sliding in normal air.

Nanocomposite TMD coatings with tailored microstructure were also deposited by Dominguez-Meister et al. [19,20], these coatings consisted in a transition metal rich layer close to the substrate, for adhesion improvement and load support, followed by a transition layer with increasing amounts of lubricious TMD phase and, finally, a functional lubricious TMD toplayer. The authors reported a good tribological response with a friction coefficient of less than 0.1 while sliding in ambient air, vacuum and dry nitrogen.

Recent studies performed by Cao et al. [21,22] on W-S-C(H) films deposited by closed field unbalanced magnetron sputtering showed substantial compositional variations as a function of the deposition parameters (target to substrate distance, working pressure). The tribological response was also dependent of the tribolayer formed in the contact, with the presence of both TMD and C phases during sliding in normal air, resulting in a friction coefficient of 0.1-0.2, and an increased presence of TMD phase when sliding in dry environments, with friction coefficients in the range from 0.01 to 0.03.

Generally, carbon-doped TMD based nanocomposite thin films have shown very promising results with a good tribological response in diverse environments. The studies by Polcar et al. [6] involving many systems (W-S-C, Mo-Se-C, W-Se-C, Mo-S-C) were mainly deposited by RF magnetron sputtering in a small deposition unit equipped with 2 cathodes, which can only fit small substrates (maximum diameter of 50mm with a thickness up to 10 mm). Moreover, there is a lack of information regarding the deposition of C-alloyed transition metal dichalcogenide coatings deposited in larger (semi-) industrial deposition units. The main challenge during the deposition of thin films containing TMDs is the compositional variation caused by the preferential re-sputtering of the chalcogen atoms from the growing film as well as the different scattering behavior of the sputtered species (e.g. W and S). Replicating the lab-scale deposition process to a larger semi-industrial scale creates the need for more detailed study due to the following:

- In an industrial deposition, parts have 3D shapes and can have big dimensions. Therefore, the target-to-substrate distance parameter can either vary significantly for the same deposition run or be much longer than in laboratory setups.

- The usage of multiple targets of C and WS_2 requires optimisation to achieve the chemical composition (previous studies report usage of a single composite target, which is not feasible on an industrial scale).
- Direct-current (DC) magnetron sputtering is often used in larger deposition units, while many of the studies previously were performed by RF magnetron sputtering. The latter requires additional instrumentation (e.g., matching network), and the deposition rates are lower, resulting in increased costs. In this context, the current density and voltage on the target can vary depending on the type of power supply used, thus, affecting the deposition process.

In an attempt to upscale the deposition process of W-S-C thin films with self-adaptive tribological response, deposition of W-S-C coatings was performed in a semi-industrial magnetron sputtering unit equipped with 4 cathodes. The main objective of the work is to gain information regarding the relationship between the process parameters and properties of the coatings. Namely, the chemical composition, (micro)structure and mechanical properties were studied as a function of selected deposition parameters. Then, a specific coating was selected for tribological studies in different testing environments, with tests carried out in normal air under different loads, at elevated temperatures, vacuum and dry nitrogen environments.

2. Experimental Methods

2.1. Synthesis of W-S-C coatings

The W-S-C thin films were deposited by closed field unbalanced magnetron sputtering in a Teer Coatings Ltd. UDP 650 unit (volume ~275 dm^3) using 4 targets with dimensions of 380 x 175 x 10 mm^3. The targets are vertically aligned on the chamber walls, the schema of the deposition unit and the configuration of the targets can be observed in Figure 1. For achieving a broad range of chemical compositions, two graphite targets (99.99 % purity) and one WS_2 target (99.9% purity) were used. In addition, a Cr target (99.9 % purity) was used for the deposition of the interlayer and gradient layer to improve adhesion. Substrates were: single crystal Si wafers, cylindrical AISI M2 steel coupons with dimensions of Ø50 x 8 mm and 10 mm 100Cr6 bearing steel balls. The M2 steel coupons were polished to R_a < 20nm using SiC papers and diamond suspension with a particle size of 3 μm. Before placing the substrates into the chamber, they were ultrasonically cleaned with acetone for 15 min and dried with air. Depositions were performed at 3 target-to-substrate distances (TSD): 10, 15 and 25 cm. The vacuum chamber was pumped down using a diffusion pump backed by a rotary vane pump; the base pressure reached before the deposition was less than 5 x 10^{-4} Pa. Sputter cleaning of the substrates and deposition of the coatings was performed in Ar atmosphere at a pressure of 0.6 Pa. The substrates were placed on holders mounted on the carousel. The carousel substrate holder was rotated at 10 rpm (single rotation), with the substrates passing in front of each target. Before deposition, substrates were sputter cleaned for 40 min by establishing plasma using pulsed-DC current (Advanced Energy Pinnacle Plus) at a bias voltage of 600 V, frequency of 250 kHz and a reverse time of 1.6 μs. Targets were also sputter cleaned before deposition for 20 min using DC power supplies (Advanced Energy Pinnacle) operated in power control mode with a power density of 2.1

W/cm^2. Cr interlayer was first deposited with a thickness of ~400 nm followed by ~100 nm gradient Cr/W-S-C layer. Total deposition time, i.e., sputtering of the interlayer, gradient layer and the coating, was 120 min. When used, substrate bias was applied using a p-DC power supply at a frequency of 250 kHz and a reverse time of 1.6 μs. No additional substrate heating was used. The deposition was performed using DC power supplies. Variation of the chemical composition was performed by setting the power density to the WS_2 fixed at a value of 2.1 W/cm^2 and changing the power density applied to the graphite targets. The power density applied on each graphite target was set to 2.6 and 3.2 W/cm^2 to achieve C content in the range of ~40-50 at. %. Additionally, a set of coatings was deposited by having the power density to each graphite target set to 2.6 W/cm^2, with 50 V bias applied to the substrate. The total number of deposited coatings was 9.

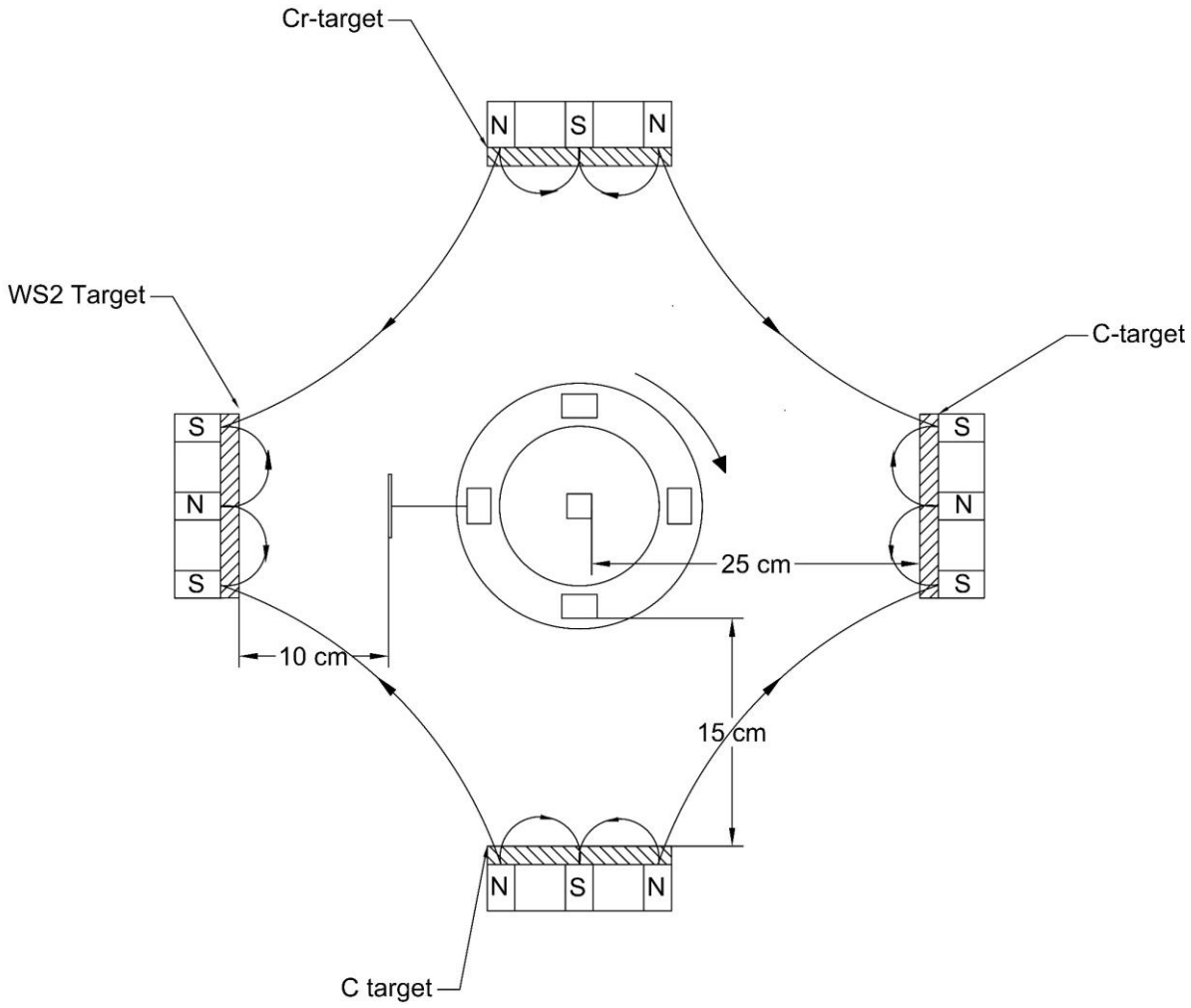

Figure 1 Schema of the deposition unit

2.2. Characterization of the coatings

Cross-section and surface microstructure were examined using a field emission scanning electron microscope (FESEM, Zeiss Merlin). Elemental composition was obtained using wavelength dispersive spectroscopy (WDS, Oxford Instruments).

The crystal structure was assessed by grazing incidence X-ray diffraction (PANalytical X'pert MRD). Cu Kα radiation was used at an incidence angle of 3°.

The hardness and elastic modulus of the coatings was measured by nanoindentation using a Berkovich type indenter (NanoTest, Micromaterials) with the load set to 5 mN resulting in indentation depths of less than 10% of the thickness of the coatings. The results presented are an average of 16 indentations. Hardness and reduced modulus of elasticity was obtained by analyzing the load displacement data using the method proposed by Oliver and Pharr [23].

Tribological testing at room temperature (RT, T=23-25°C, relative humidity RH~30-45%) was performed on an in-house made unidirectional pin-on-disk tester under loads of 5 (initial maximum contact pressure of ~820 MPa) and 35 N (initial maximum contact pressure of ~990). It should be noted that tests were also performed at fixed RH of 23 % and 75 % (see Figure S1 in the supplementary information). The only difference observed was related to the running-in period. The steady-state response was quite similar for both RHs. Therefore, the significant effects of RH during these tests are not expected. Increasing the load was considered as these coatings often show non-Amonton tribological behavior (decrease of the friction coefficient as the load is increased [24]). Bearing steel balls (DIN 100Cr6) with a diameter of 10 mm were used as counterbodies. The testing under a load of 5 N was limited to 10^4 and 5 x 10^4 cycles. The test under increased load (35 N) was performed for only 10^4 cycles to prevent the complete removal of the coating.

Tribological tests at elevated temperatures (ambient air) were performed using a high temperature unidirectional pin-on-disk tester (CSM Instruments). The dry sliding tribological testing was performed with a normal load of 5 N (initial maximum contact pressure of ~1154 MPa, at RT) with 6 mm 100Cr6 ball used as a counterbody. The testing temperature was set to 100, 200, 300 and 400°C. The maximum temperature was set at 400°C since previous studies have shown that coatings with similar composition and microstructure can provide lubrication

up to 400 °C [25]. Steel based material instead of more thermally stable ceramic-based material was chosen as counterbody, because it can better mimic the materials encountered in real applications (parts in combustion engines, workpieces in metal forming, sliding components in injection molding machines and sliding components in the aerospace industry). Additionally, there is more data regarding the performance of self-lubricating thin films tested against bearing steel counterbodies, hence a comparison of the performance can be made more easily. At 400°C, the hardness of the steel is still ~50 HRC. The duration of the test was limited to 5000 cycles. A test was also performed at room temperature with the other testing conditions kept the same to have a better comparison between RT testing and high-temperature testing.

Tests in high vacuum and nitrogen atmosphere were performed using a unidirectional pin on disk tester (same equipment used for the RT testing) placed in a vacuum chamber pumped by a turbomolecular pump, backed by a dry scroll vacuum pump. Vacuum tests were performed at pressures lower than 10^{-3} Pa. Tests in nitrogen were performed by pumping the vacuum chamber to a pressure of ~10^{-3} Pa, and then, filling the chamber with high purity (99.999%) nitrogen to a pressure of 10^4 Pa. Initial vacuum testing was performed against 10 mm 100Cr6 counterbody under a load of 2 N (initial maximum contact pressure of 605 MPa). Additional tests in a vacuum and dry nitrogen were performed against W-S-C coated 10 mm 100Cr6 balls, with a load of 2 N. Testing was performed for 10^4 sliding cycles, unless otherwise noted. The testing parameters are summarized in Table I.

All tests were performed at a sliding radius of 10-15 mm, with the rotational speed being adjusted to obtain a sliding speed of 0.1 m/s.

Table I Parameters for the tribological testing

Test parameters	Room temperature testing
Load [N]	5 N, 35 N
Speed [m/s]	0.1m/s
Duration [Number of cycles]	10000, 50000[a]
Counterbody	10 mm 100Cr6 balls
Test parameters	High temperature testing
Load [N]	5 N
Temperature	RT, 100, 200, 300, 400
Speed [m/s]	0.1m/s
Duration [Number of cycles]	5000
Counterbody	6 mm 100Cr6 balls
Test parameters	Vacuum and dry N_2 testing
Load [N]	2 N
Speed [m/s]	0.1m/s
Duration-Number of cycles	10000
Counterbody	10 mm 100Cr6 balls[b] and W-S-C coated 10 mm 100Cr6 balls

[a] Tested only with 5 N

[b] Only in vacuum

Before testing, the coated disks and the counterbodies were ultrasonically cleaned for 15 min using ethanol, rinsed with acetone and dried with hot air.

3D profilometry of the wear scars was performed using a Zygo NewView ™ 7300 scanning white light interferometer. Four cross-sections obtained at a different location on the circumference of the wear scar were used for wear volume calculation by multiplying the cross-sectional area with the circumference of the scar. Wear volume of the spherical counterbodies was considered to be a spherical cap and it was calculated using the following expression:

$$V = \left(\frac{\pi h}{6}\right)\left(\frac{3d^2}{4} + h^2\right) \quad (1)$$

Where h is the height of the cap calculated as:

$$h = r - \sqrt{r^2 - \frac{d^2}{4}} \quad (2)$$

The scar diameter d is obtained from the 3D white light interferometer and r is the radius of the ball. Using the wear volume, the specific wear rate was calculated (Eq. 3).

$$W_r = \frac{V}{Fs} \quad (3)$$

Where F is the normal load and s is the sliding distance. At least two repetitions were performed per coating tested.

Raman spectroscopy on the wear scars was performed using a 532 nm laser (XploRA, Horiba) with the range of Raman shift values set to 100-2000 cm^{-1} and the power to the laser and acquisition time (120s) adjusted in order to prevent damage to the coatings. A 100x objective (numerical aperture of 0.9) was used, resulting in a spot size of ~ 1-2 μm.

The wear tracks were also studied using SEM and energy dispersive spectroscopy (EDS). The analysis was performed with an accelerating voltage of 15 kV.

3. Results and discussion

3.1. Elemental composition

The list of coatings as well as their elemental composition, thickness and deposition rate are summarized in Table II. The carbon contents were in the range of 38-55 at. % and compositional variations were observed depending on the target-to-substrate distance (TSD), bias voltage and power applied to the graphite targets. The thickness of the coatings deposited without substrate bias was ~2µm for deposition distances up to 15cm, with a reduction to ~1.6 µm for the coatings deposited at a distance of 25cm. Usage of substrate bias resulted in lower thicknesses, at constant TSD, which can be a result of material removal caused by the continuous Ar^+ ion bombardment of the substrates during deposition and overall densification of the coatings [26].

Table II List of coatings deposited, deposition parameters and elemental composition

Coating	Target to substrate distance (cm)	Substrate bias (V)	Power applied to targets (W/cm^2)		Elemental composition (at. %)				S/W ratio	Thickness (µm)/Deposition Rate (nm/min)
			WS_2	C (x2)	C	S	O	W		
WSC1-10	10	0	2.1	2.6	44.0	28.5	4.9	22.6	1.26	2/16.7
WSC1-15	15	0	2.1	2.6	40.2	32.5	5.2	22.1	1.47	2.3/19.2
WSC1-25	25	0	2.1	2.6	38.1	35.1	5.8	21.1	1.66	1.6/13.3
WSC2-10	10	50	2.1	2.6	45.8	25.1	3.1	26.0	0.96	1.8/15
WSC2-15	15	50	2.1	2.6	48.2	24.0	2.8	25.0	0.96	1.7/14.2
WSC2-25	25	50	2.1	2.6	40.8	32.7	2.8	23.7	1.38	1/8.3
WSC3-10	10	0	2.1	3.2	57.6	20.1	2.4	20.0	1.01	2/16.4
WSC3-15	15	0	2.1	3.2	52.2	26.1	1.5	20.2	1.29	2/16.3
WSC3-25	25	0	2.1	3.2	53.0	27.5	2.4	17.1	1.61	1.6/13.1

The S/W ratio shows increasing trends as the TSD is increased (see Figure 2). Similar trends were also observed by Cao et al. [22], where a similar deposition unit was used. However, they reported lower values of S/W ratio (below 1) for distances up to 15 cm. During synthesis of TMD containing coatings by sputtering techniques, the sub-stoichiometry with respect to sulfur (S/W < 2) is generally a result of 2 processes: (i) gas phase scattering of the sputtered atoms, during their travel towards the substrate and, (ii) preferential resputtering of the chalcogen atom from the growing film [27]. At small TSD distances, the preferential resputtering of the chalcogen atoms from the growing film seems to have a major effect on the composition. In fact, for the discharge pressure used in the deposition (0.6 Pa), the mean free path of the particles is still very high, only being expected a few collisions during the interelectrode sputtered atoms trajectories; preferential resputtering should be, then, responsible for the lower S/W ratios.

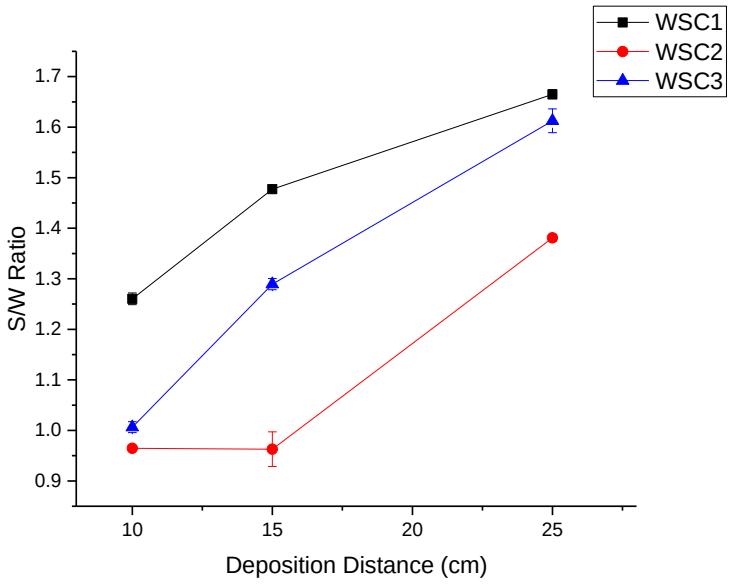

Figure 2 S/W ratio as a function of deposition distance

The reduction of S/W ratio as a result of negative substrate bias is a well-known phenomenon; by using p-DC bias on the substrates, the substrates are continuously bombarded by Ar^+ ions.

Therefore, preferential sputtering of the lighter element, S, in relation to W occurs, which is often reported in the literature [28], resulting in a reduction of the S content in relation to W content. A similar trend is observed with the increase of the power to the graphite targets, which resulted in increased target voltage and current. Such effects will contribute to the increase of the energy and number of neutral Ar atoms reflected on the target, produced by charge exchange collisions in the discharge cathode sheath. Reflected neutrals will bombard the growing film promoting the preferential sputtering of S in relation to W, which explains either the sub-stoichiometry (S/W ratios < 2) of all the deposited films or the lower S/W ratio when the C target power was increased.

The increase of the TSD has a marked influence on the S/W ratio due to the increasing importance of the particle collisions in the interelectrode space. On the one hand, reflected neutrals will be progressively thermalized having less and less influence on the resputtering effect of the growing film. Consequently, S will be preferentially sputtered from the growing film in a lesser amount, leading to a higher S/W ratio. On the other hand, the increasing number of collisions will make the deflection in the trajectories of both W and S sputtered atoms less different. For low target to substrate distances, as the number of collisions is low, W atoms being much heavier will not be scattered as a result of collisions with the Ar atoms present in the chamber, resulting in more straight traversing paths and subsequent W enrichment. S atoms are much lighter and will scatter more during their travel resulting in S depletion. However, when that distance increases, a higher number of collisions occur, with a consequent loss of energy of the sputtered atoms, being the diffusion mechanism in the transportation process more and more important. Therefore, the transport of sputtered species becomes similar, independently of their mass. As a consequence, the arrival rate of both W and S atoms to the

growing film does not differ so much in relation to the sputtering rates in the target, giving rise to higher S/W ratios as the substrate to the target distance increases.

The effect of the increase of the target to substrate distance on the S/W ratio for coatings deposited using substrate bias is not so strong as in unbiased coatings (see Figure 2). From the two effects above described for unbiased coatings, the attenuation of the resputtering effect should not be considered in the analysis since, in this case, bombarding species are the Ar ions extracted from the discharge and accelerated by the negative bias potential applied to the substrate. Although challenging to analyze, small variations can be expected since the number of bombarding ions can vary with the position of substrates inside the deposition chamber. As the system works in unbalanced mode, magnetic field lines between cathodes can originate zones of higher density plasma in the discharge, affecting the ion current to the substrate. This is a possible explanation for the same values found for S/W for positions at a substrate to target distances of 10 and 15 cm. As for the other coatings, a small increase in the S/W ratio would be expected for the 15 cm of TSD. This can only be understood if a slightly higher bombardment occurs at that substrate position, which is possible if a higher plasma density exists nearby.

Considering the elemental composition achieved for the deposited films, several factors were found to affect the composition of the films, with the TSD playing a major role. The total amount of power applied to the targets also resulted in compositional variation. Usage of substrate bias for deposition of thin films is an excellent alternative to improve the overall tribo-mechanical properties, but, for this particular type of coatings, its usage will significantly hinder the lubrication properties as the coating will be depleted of sulfur.

3.2. Microstructure and crystallinity

Carbon addition to TMD based coatings results in the densification of the microstructure compared to the typical porous microstructure of pure sputtered TMD based coatings [6]. All cross-sections presented in Figure 3 show dense morphologies, although a slight decrease in the compactness can be perceived when TSD increases, particularly for the 25 cm value, the coating having the lowest amount of C (38 % at.) and the highest S/W ratio (~1.6) for which some porosity and signs of columnar growth can be observed (Figure 3 c)). As explained above, these coatings deposited with increasing TSD are submitted to lower bombardment with its consequent detrimental effect on their density.

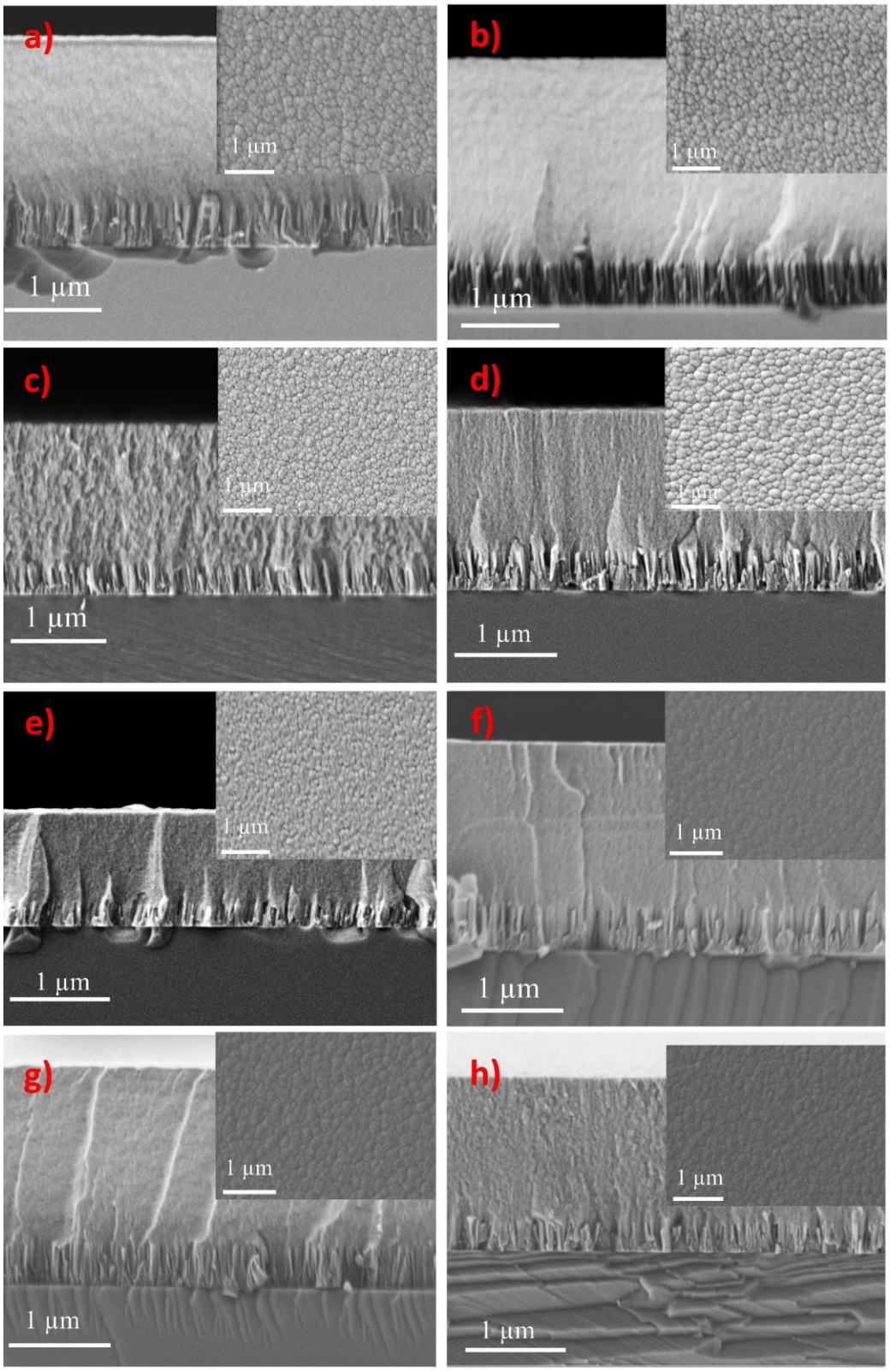

Figure 3 SEM micrographs of the cross-sections of as deposited coatings with the insets showing the top surface morphologies a) WSC1-10, b) WSC1-15, c)WSC1-25, d)WSC2-15, e)WSC2-25, f) WSC3-10, g) WSC3-15, h) WSC3-25

The top surface morphology of the coatings showed a cauliflower structure, which is typical of magnetron sputtered TMD thin films containing carbon.

The GIXRD patterns shown in Figure 4 indicate X-ray amorphous structures with a broad peak at 2θ~30-40° with a tail towards higher angles. This broad peak is often related to a (100) reflection of WS_2 at 33° with the tail representing turbostratic stacking of (10L) planes [29]. However, the peaks related to tungsten carbide are positioned in this region, too (see ref. [30,31]), making the interpretation of the pattern difficult. Although we cannot exclude the presence of WS_2 or WC crystals, their grain size would be below the detection limit of XRD (i.e., lower than 3-4 nm).

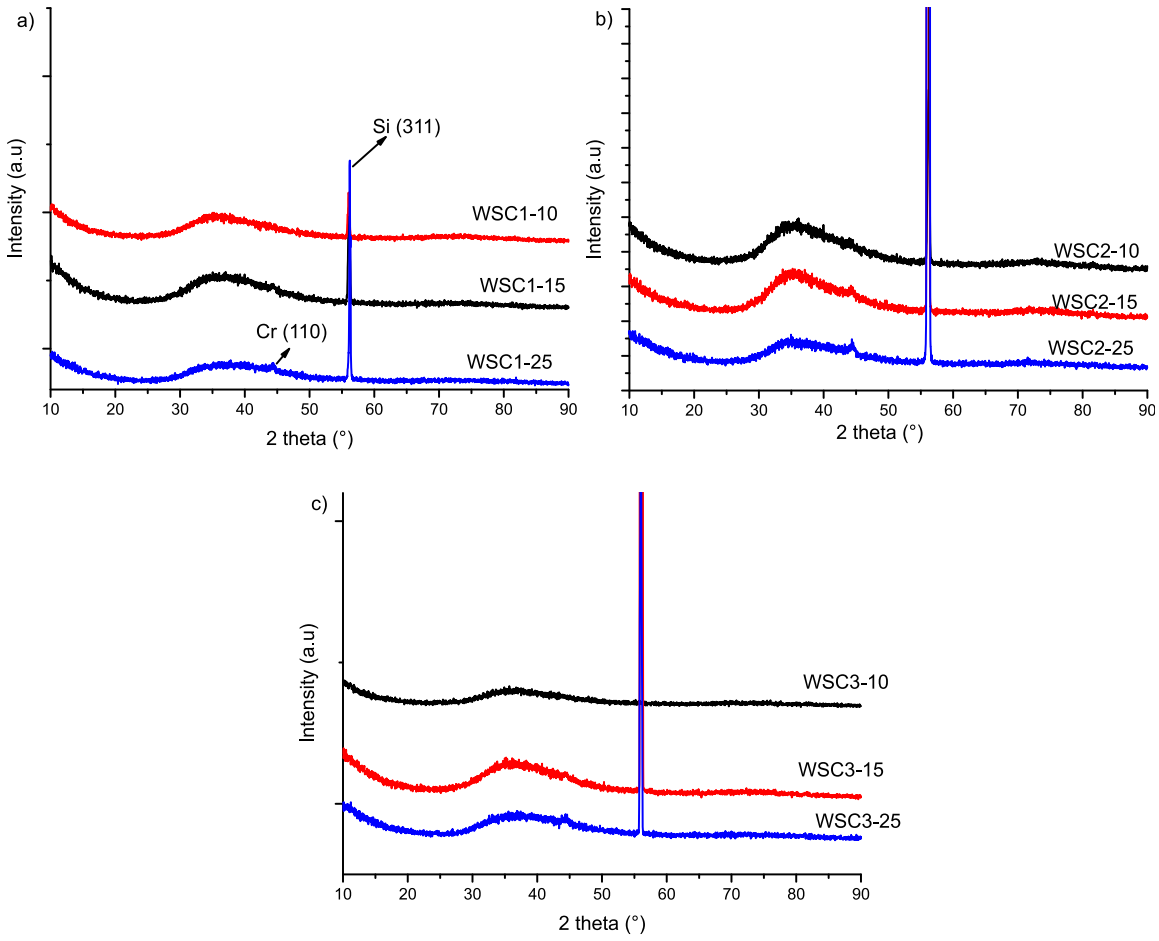

Figure 4 GIXRD patterns for: a) WSC1, b) WSC2, c) WSC3

3.3. Mechanical properties

Hardness (H) and reduced modulus of elasticity (E*) values from nanoindentation experiments are shown in Figure 5 a) and b), respectively. The hardness is reduced when the target to substrate distance is higher. It is worth mention that non-hydrogenated DLC coating deposited in this equipment at the target to substrate distance of 15 cm, with similar power applied to the graphite targets and substrate bias of 50 V, yielded a hardness of ~13-15 GPa [32]. Therefore, an increase in hardness with higher carbon content is expected. The presence of tungsten carbides could further enhance the hardness [33], and for films with a lower S/W ratio, there is more W available for the formation of W-C phases. On the other hand, the high content of sulfur

in amorphous films or nanocrystalline WS_2 phases leads to hardness reduction. Finally, more compact films achieved at the lower substrate to target distances are expected to be more resistant to the indenter penetration, which would result in an increase of the hardness.

As expected, the softer coating is the one deposited without substrate bias and lower carbon content for the same substrate to target distance. The factors influencing the hardness have already been discussed; the films deposited with substrate bias are more compact and have lower S/W ratios resulting in hardness increase. Similarly, the films deposited with a higher power in the C targets have a higher content of the harder a:C phase. Thus, their hardness exceeds the ones prepared with substrate bias and lower C content.

Reduced elastic modulus values follow the trends observed for hardness values. The values of H/E*, representative of elastic strain to failure [34], and H^3/E^{*2}, which is proportional to the resistance to plastic deformation, are often related to the wear behavior of the coatings with lower values for reduced modulus of elasticity desirable [35]. H/E* ratios are in the range of 0.054-0.081 with lower values for a longer target to distance; as an example, WSC1 coating deposited at 10, 15 and 25 cm has values of 0.08, 0.081 and 0.069 respectively. The values of H^3/E^{*2} were in the range of 0.018-0.057 and similar trends were observed as for the H/E* ratio.

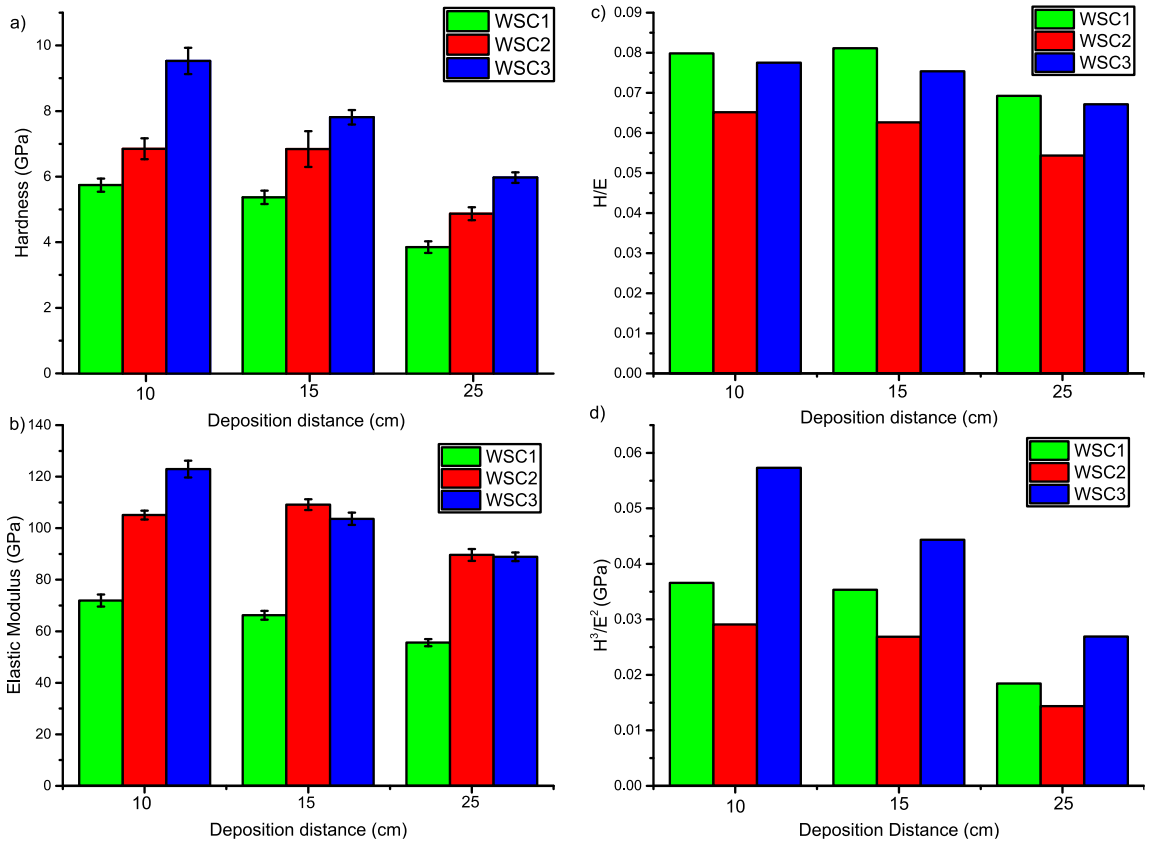

Figure 5 a) Hardness, b) Elastic Modulus, c) H/E and d) H3/E*2 of the coatings*

3.4. Tribological properties

The selection of the coating for the tribological testing was based on the best compromise among various relevant parameters, such as: overall S content, S/W ratio, hardness, cross-sectional morphology, H/E* and target-to-substrate distance. For tribological testing, the WSC1-15 was selected due to moderate hardness (~5.7 GPa), a moderate S/W ratio (1.47), a high amount of the lubricious WS_2 phase (only 40 at. % of C and a total of ~32 % of S) and among the highest value for H/E* parameter, which is known to be related with the tribological performance. Moreover, this TSD is generally used for the deposition of coatings in this deposition equipment.

3.4.1. Influence of the normal load

The evolution of the friction coefficient can be seen in Figure 6 a). The test performed under a 5 N load showed a friction coefficient of ~0.15 at the start of the test, followed by a decrease to ~0.1 in the initial 2500 cycles. After an initial testing phase, an increase of friction is observed with value as high as 0.25 after 40000 cycles, followed by a drop to a value of ~0.17. Testing under higher load (35N) resulted in a much lower coefficient of friction, starting at 0.05 with a steady increase towards a final value of ~0.07, with an average value of 0.06. Similar trends (non-Amonton behavior) were also observed in previous studies [6]. Specific wear rates calculated after the tribological tests can be seen in Figure 6 b). The coating tested with 5 N of load (5 x 10^4 cycles) showed an average value of ~3 x 10^{-7} mm^3 N^{-1} m^{-1}. Testing with 35 N resulted in lower wear rates for the disk with a value of ~1.0 x 10^{-7} mm^3 N^{-1} m^{-1}. Higher counterbody wear was observed for the 100Cr6 balls from the tests under the load 35N (~10^{-8} mm^3 N^{-1} m^{-1}) compared to the ones tested with 5 N load (~8 x 10^{-9} mm^3 N^{-1} m^{-1}).

Raman spectroscopy was performed on the wear scars of the disks as well as on the counterbodies. For the coating tested under 5 N load, the analysis was performed after the test with 5 x 10^4 cycles. The as deposited coating does not show any peaks related to WS_2, with the most prominent peaks being D and G peaks with location and intensity typical for amorphous carbon. Raman spectra on the disk track after testing with 5 N of load did not show any significant changes, the main feature observed was the D and G peaks related to the a-C phase with very similar intensities compared to the as deposited coating. The Raman spectroscopy performed on the tribolayers formed on the bearing steel ball show strong intensities related to graphitic carbon (see Figure 6 c)). The Raman spectroscopy performed on the wear debris revealed the presence of tungsten oxides (Raman shift values of ~800 and ~970 cm^{-1}) and graphitic carbon. On the other hand, the analysis performed on the tribolayers formed on the

disk track, and the ball scar, after testing with 35 N load, shows intensities at Raman shift values of ~350 and ~417 cm^{-1}. Tungsten disulfide has two distinct Raman peaks in this region; the first one is at 350 cm^{-1} (representing the in-plane phonon mode $E^1_{2g}(\Gamma)$) while the second peak is located at 417 cm^{-1} (related to the out of plane phonon mode $A_{1g}(\Gamma)$) [36]. As a reference, a Raman spectrum from pure sputtered WS_2 was also plotted. These changes in the Raman spectra can be attributed to the presence of crystalline WS_2 on both surfaces in the sliding contact. The presence of crystalline WS_2 on the sliding surfaces can be associated with the observed reduction in friction [37]. The drop in friction as the load is increased can be associated with the presence of a low shear strength tribolayer rich in WS_2; increasing loads facilitate the formation of this tribolayer. Furthermore, TMD containing coatings are known to provide a lower coefficient of friction with increased loads (see ref [38–40]). A drop in the coefficient of friction with increased loads was also observed in previous studies on lab-scale deposited W-S-C coatings [24]. A recent molecular dynamics (MD) study [41] had shown that there is an energy threshold that needs to be achieved to trigger amorphous to crystalline transition in MoS_2. In our case, the usage of increased load can significantly raise the energy input at the sliding interface, providing enough energy to induce increased crystallization of the WS_2 phase, resulting in the formation of a low friction tribofilm. Based on these results, the tribological behavior (under standard laboratory air) of this coating is mainly governed by graphitic tribofilms during testing with low normal loads (e.g 5 N). Increasing the normal load (35 N in our case) causes the formation of a WS_2 (very likely due to higher energy input in the contact) with higher crystallinity. The presence of WS_2 in the sliding interface further facilitates the lubricity, which is evident by the drop in the coefficient of friction.

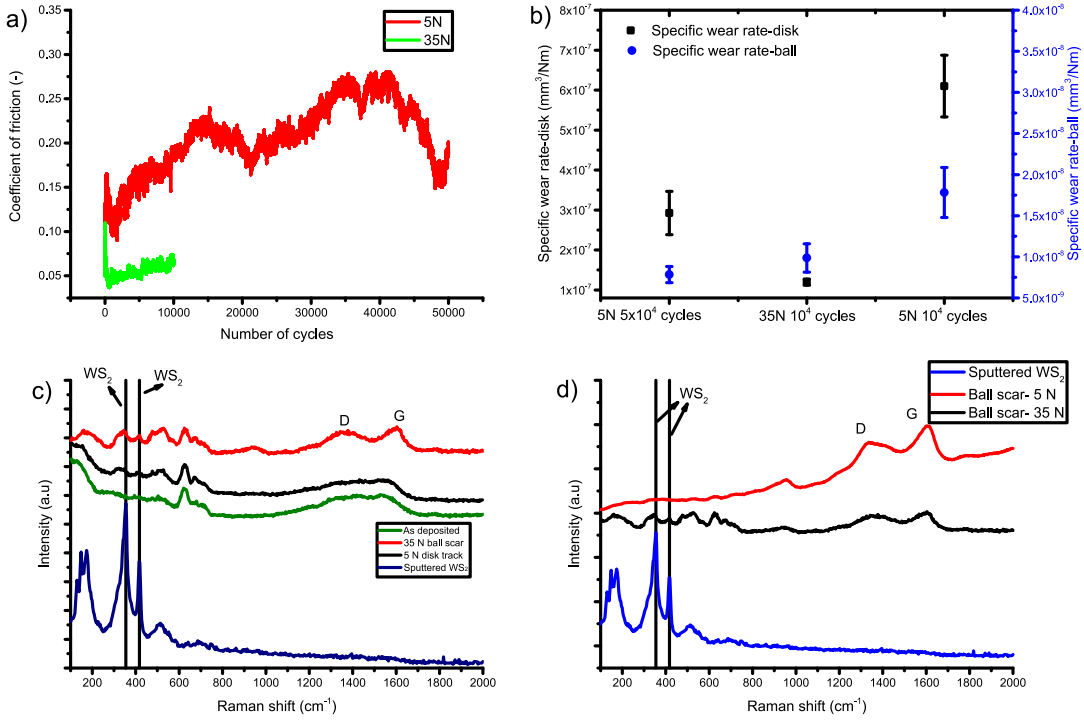

Figure 6 Result from the tribological testing in normal laboratory air: a) evolution of friction coefficient, b) specific wear c) Raman analysis of the wear tracks d) Raman analysis of the ball scars

3.4.2. Influence of testing temperature

The tribological behavior of the coatings was tested at different temperatures from 100 to 400 °C. Figure 7 a) shows the evolution of the friction coefficient as a function of the number of sliding cycles. Running-in phase with steadily decreasing coefficient of friction from an initial value of 0.05 was observed at 100 °C; at about 1500 cycles, the coefficient of friction stabilized at a value as low as 0.01. The running in period was much shorter for the tests performed at 200-400 °C and the steady state regime is observed after 500 cycles. Average friction coefficient values calculated from the last 2500 cycles are shown in Figure 7 b).

In terms of wear, the coating shows increasing wear with testing temperature (Figure 7 c)). The wear in the counterbody follows similar trends as the disk wear for testing at temperatures up

to 200 °C. Surprisingly, at the highest testing temperatures, no wear was detected on the counterbodies, due to material transfer from the coating (see for example, Figure S3 and S4 in the supplementary information). Similar tribological behavior of W-S-C coatings deposited in lab-scale equipment by RF magnetron sputtering with similar C content, and slightly lower S/W ratio, was also observed by Polcar et al. [25].

Again, Raman spectroscopy was used to investigate worn surfaces; an example is shown in Figure 7 d) (testing temperature of 100 °C). Raman spectroscopy performed on the tribofilms, at locations similar to the patches of material shown at location 1 on Figure 8 b), formed after sliding at elevated temperatures show clear contributions of the WS_2 phase responsible for a very low value of the coefficient of friction. It should be noted that Raman performed in the areas showing only shallow abrasive marks revealed a spectrum quite similar to the as-deposited one. The wear track after testing at 400 °C was also analyzed using SEM. An overview of the scar is shown in Figure 8 a). No signs of delamination indicate excellent adhesion of the coating to the substrate. The wear track was mostly smooth with shallow abrasive marks and areas with patches of adhered material. Higher magnification imaging and energy-dispersive spectroscopy (EDS) was performed on these patches, see Figure 8 b). EDS performed on the adhered material (area 1) showed a significant amount of oxygen and a small but measurable amount of iron, the latter originates from the counterbody. EDS performed in area 2 showed a higher amount of C (71 at. %) and lower S/W ratio (1.2, compared to 1.47 from the as deposited state); however, there were no vestiges of iron and a meager amount of oxygen.

Two main effects should be considered to understand the effect of temperature on the friction behavior. Firstly, heating to temperatures higher than 100 ºC allows drying of the atmosphere around the testing rig, avoiding the detrimental effect of humidity in increasing the friction.

Secondly, the increased temperatures facilitate the formation of crystalline WS_2 phase [41], and decrease its shear strength, which further contributes to the friction reduction. Raman spectroscopy performed on the tribofilms also shows the presence of graphitic carbon as a consequence of the structural transformation of the a-C phase. The presence of graphitic carbon, a very soft phase, in the tribofilms is likely the cause of the increased wear of the coating. Although carbon-based material was detected in the tribofilms, its role towards the frictional response is mainly related to the load-bearing capacity. It should be noted that non-hydrogenated graphitic carbon is unable to provide friction reduction at elevated temperatures due to the lack of water vapour needed as an intercalating agent [42]. Increased coefficients of friction were often observed for non-hydrogenated a-C coatings during elevated temperature testing (see, for example, Ref. [43,44]). Furthermore, the Raman signal can also originate from volumes below the lubricious tribofilms. Considering a very low coefficient of friction, the tribological response is mainly governed by the crystalline WS_2 formed during the testing, while the carbon phase provides the load-bearing capacity. The Raman spectroscopy performed on the wear debris (not shown) indicated D and G peaks typical of graphitic nature with very high intensity, together with a small WO_3 contribution at Raman shift value of ~800 cm^{-1}.

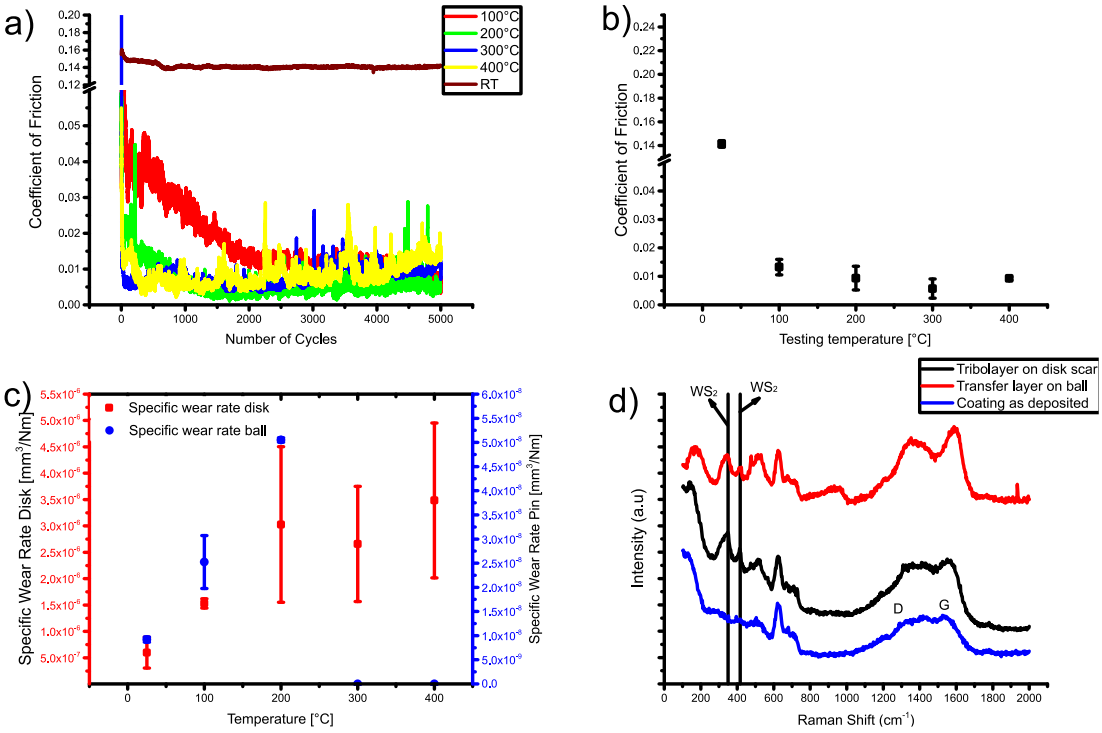

Figure 7 Results from the tribological tests at elevated temperatures: a) Evolution of friction coefficient as a function of number of cycles, b) average friction coefficient as a function of testing temperature for the last 2500 cycles, c) specific wear rate of the pin and the coated disk as a function of testing temp d) Raman spectra obtained from the disk and ball after testing at 100°C.

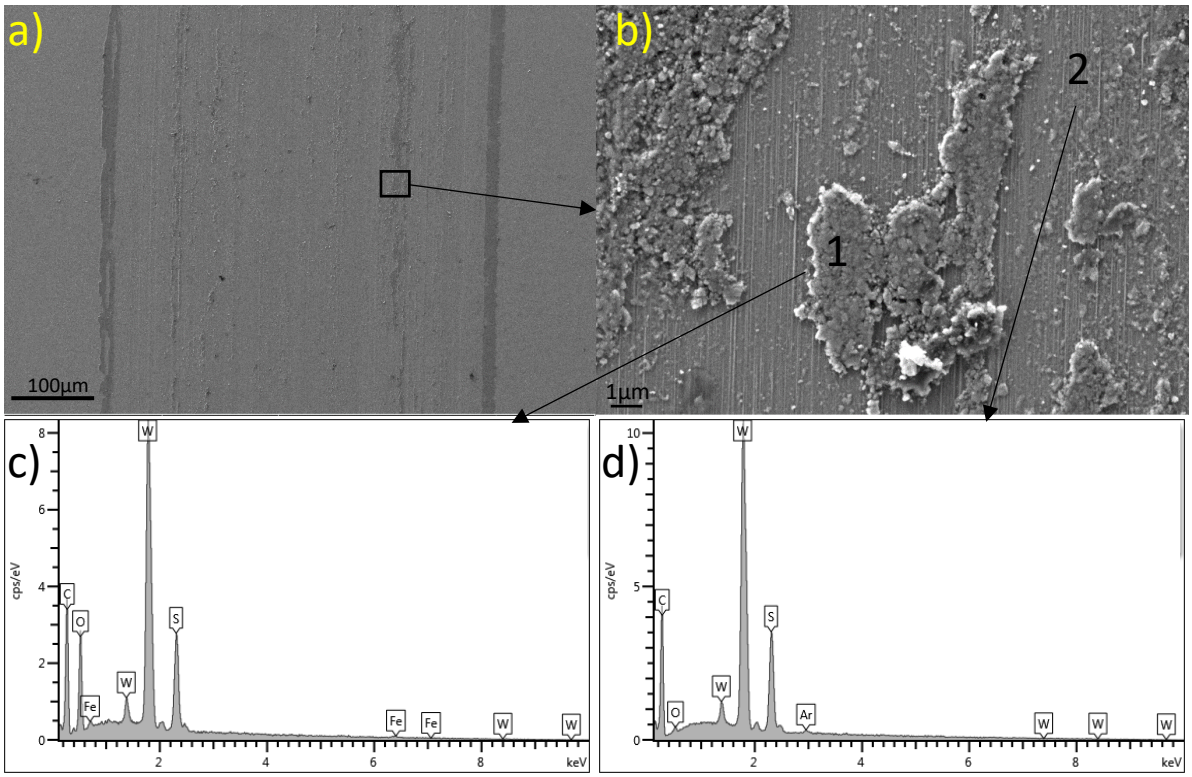

Figure 8 SEM imaging performed on the coating tested at 400°C: a) overview, b) higher magnification detail c-d) EDS spectra

3.4.3. Tests performed in vacuum and dry nitrogen

Initial testing in vacuum was performed against a 100Cr6 bearing steel counterbody under a load of 2 N (see Figure 9). The very low friction coefficient of ~0.01-0.02 was measured for the first 100 cycles after which a significant increase in the friction coefficient occurred with a final value of 0.4-0.5 at 800 cycles when the test was stopped. 3D profilometry performed on the ball counterbody revealed significant wear with a wear scar diameter of ~0.8 mm. On the other hand, 3D profilometry on the wear track of the disk did not show any wear with a significant presence of transferred material.

Considering the significant amount of wear of the bearing steel counterbody, with an indication of material transfer to the coated disk, it is clear that 100Cr6 bearing steel is not an appropriate sliding partner to achieve low friction. Therefore, the balls were also coated with the same coating as the disks and the sliding tests were performed with a load of 2 N in a vacuum and a dry nitrogen environment. For the vacuum tests, the coefficient of friction was very low in the initial 1000 cycles with values below 0.01. Then, a spike in the friction appeared. Periodic spikes in friction to values up to 0.4 were followed by drops to low values in the range of 0.01-0.02 until the end of the test. These spikes are a clear indication of coating failure and an optical micrography showed zones where the coating flaked off at the counterbody revealing the steel surface. The delamination was limited only to the coated ball; the integrity of the coating deposited on the disc was preserved with maximum wear depth lower than the thickness of the coating. Specific wear rates for both triboelements were quite high, 2.5×10^{-5} and 1.3×10^{-6} $mm^3\ N^{-1}\ m^{-1}$ for the disk and the pin, respectively.

Tests performed in dry nitrogen showed a much more stable friction coefficient. Starting at rather low values of ~0.01, the coefficient of friction continuously increased up to values of 0.03-0.04 after around 1000 cycles. For the remaining time of the test, the friction coefficient fluctuated within values between 0.02-0.04, values slightly higher than those found in tests performed in a vacuum (not considering the spikes). Only sporadically, friction spikes occurred. The coatings showed lower wear compared to the tests performed in a vacuum with values of 2.4×10^{-7} and 3.7×10^{-8} $mm^3\ N^{-1}\ m^{-1}$ for the disk and the pin, respectively. Raman spectroscopy was performed on the triboelements after testing under dry N_2 and vacuum environment (see Figure 10). The tribolayers analyzed after testing with presented intensities in the regions related to WS_2 (~350 and 417 cm^{-1}) as well as intensities related to carbon-based phases (1200-1700

cm^{-1}). Based on these results, the tribolayers are composed of C-based and TMD-based materials.

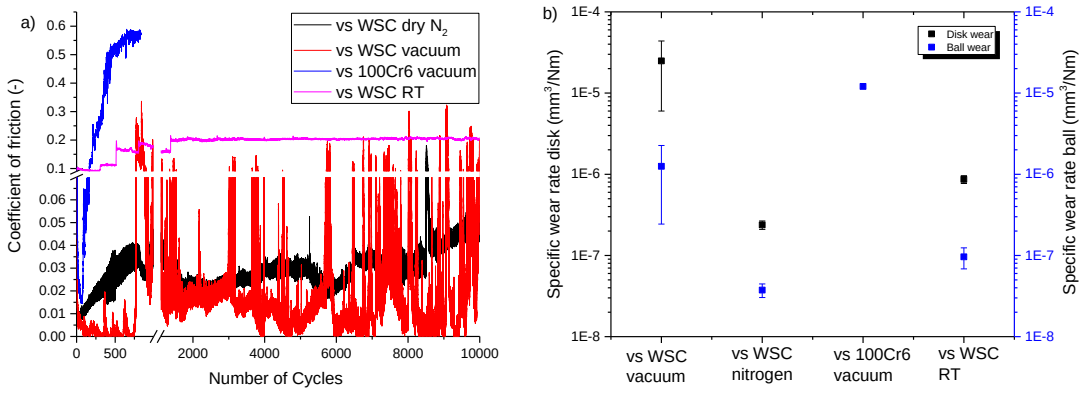

Figure 9 Results from the testing in vacuum and dry N2 environments a) coefficient of friction b) specific wear rate

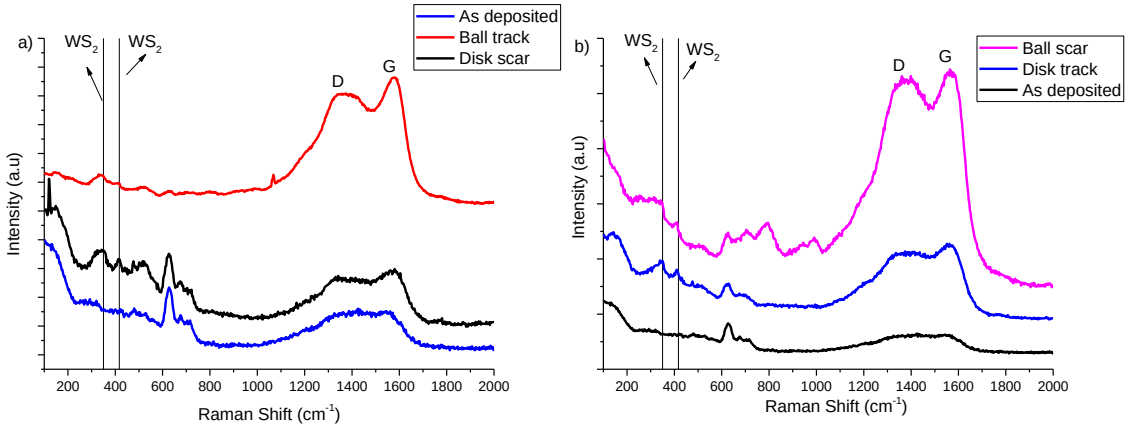

Figure 10 Raman spectroscopy performed after testing against W-S-C coated balls a) Dry N_2 environment b) vacuum environment

SEM was also performed on selected wear tracks (see Figure 11) from the testing performed in dry N_2 and vacuum. The disc track after testing with 2 N load against 100Cr6 counterbody in a vacuum can be observed in Figure 11 a,b). Lower magnification overview of the scar shows the

presence of material transfer (darker regions in Figure 11 a)). Two regions were selected for EDS analysis (spots 3 and 4 in Figure 11 b)). The EDS analysis performed in the darker region (spot 3) resulted in 15% at. of O, 5% at. of Fe, 2 % at. of Cr, with the rest being a mixture of W, C and S, indicating transfer of ferrous material from the steel counterbody. Compared to the composition obtained from the analysis done on the brighter areas of the scar (spot 4), darker patches, also contain more C and O. Considering the high coefficient of friction and the preferential wear of the steel counterbody, it is very likely that the friction is governed by the non-hydrogenated carbon phase, which is known to be unable to provide friction reduction unless species that can passivate the carbon atoms (e.g. water vapour, hydrogen) are available [45]. The presence of a non-hydrogenated carbon phase on the sliding interface, unlike during sliding in air, is disadvantageous during sliding in a vacuum. Furthermore, as iron-based material is transferred on the disk, the interface between both counterbodies will be of a metal-to-metal type, which can have strong adhesion in a vacuum resulting in a high coefficient of friction and wear of the counterbody [46]. Comparing the tests at high temperature and in a vacuum, it is very likely that crystallization of the WS2 at elevated temperatures is occurring quite fast and the friction is governed by WS2 rich tribofilm, while the effect of the carbon phase is not as negative during elevated temperatures testing compared to the vacuum testing. For example, Krumpiegl et al [43] observed considerably worsened performance of non-hydrogenated a-C coatings during testing under vacuum compared to elevated temperature.

SEM was also performed on the wear track after testing with 2 N of load against W-S-C coated ball in a vacuum environment (Figure 11 c)). Only minimal amount of material transfer is visible compared to the test performed against 100Cr6 ball. EDS performed on one of these areas (spot 5, Figure 11 d)), also showed the presence of Fe (5 at. %) in addition to an increased amount of

oxygen, again indicating material transfer from the ball. Cr was also detected (up to 1% at.), and, in this case, it can originate from the interlayer of the film deposited on the counterbody, as the coating of the ball was worn through during the test. Finally, SEM was also performed on the scars after testing in a nitrogen environment. The main difference that was observed is the presence of a much narrower wear scar (compare Figure 11 a,c) and Figure 11 e). Smooth darker patches were also seen, aligned in the direction of sliding. EDS was performed on the brighter and darker areas of the scar, but no significant difference was observed.

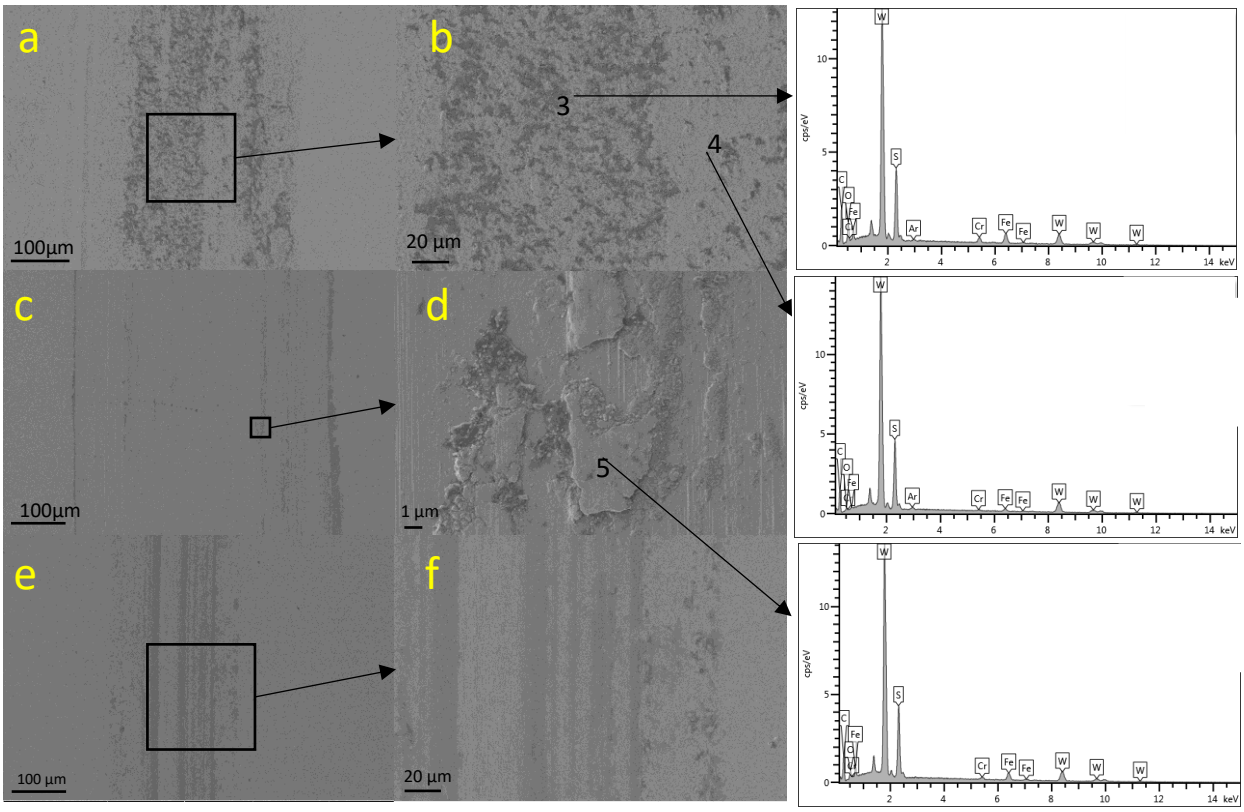

Figure 11 Figure 10 SEM micrographs of the disk wear scars after testing: a-b) 2N vs 100Cr6 in vacuum, c-d) 2N vs WSC coated ball in vacuum, e-f) 2N vs WSC coated ball in nitrogen

A significant difference can be observed for the tribological response of the WSC-WSC tribopair tested in a vacuum and dry nitrogen environments. Coatings with similar composition

were also tested in a vacuum and dry N_2 against steel counterbodies in the work of Voevodin et al. [10]. Contrary to this study, for coatings with at least 22. % at. of sulfur they observed very low friction in both dry N_2 and vacuum. In that work, the coatings that provided lubrication in dry N_2 had similar performance in a vacuum. The most probable reason for this behavior should be the different S/W ratio, although other parameters, such as the level of crystallinity of the films should not be disregarded [47]. Unfortunately, neither the crystallinity nor the S/W ratio can be indexed to the particular film, which was tested by Voevodin et al. in the conditions herein used. The worsened tribological response in a vacuum, for the coatings having low sulfur content, was attributed to the inability of the non-hydrogenated amorphous carbon to provide lubrication in a vacuum and dry N_2 environments.

Extensive testing of TMD coatings alloyed with carbon was also performed in dry environments (N_2, dry air, Ar), against steel counterbodies [48–50]. The coatings having a similar chemical composition to the one presented in this study, have shown very good tribological performance. The reduction of friction and wear in these cases was attributed to a TMD tribolayer, protected from environmental attack with its basal planes oriented in the direction of sliding. The influence of the carbon phase was mostly related to the hardness improvement; during sliding it was preferentially removed from the sliding interface. Comparing those results with the ones presented here, the coefficient of friction values (between 0.02-0.04) and specific wear rates for the disk (10^{-7}-10^{-6} mm^3/Nm) are quite similar, indicating that the friction reduction mechanism is similar. Indeed, Raman spectroscopy performed on the triboelements showed the presence of crystalline WS_2 on the sliding surfaces, while the debris was rich in graphitic carbon indicating that the C-phase is removed from the contact.

Considering the results from the testing performed in a vacuum, the mechanism proposed for friction and wear reduction in dry atmospheres (e.g dry N_2) might not be valid. The coefficient of friction values when 100Cr6 bearing steel balls slide against the W-S-C coating are very similar to the values for non-hydrogenated carbon coatings sliding against steel counterbodies in a vacuum (see Ref. [45,51]). Considering the similarities of the tribological response of the tribopair in a vacuum with the behavior of non-hydrogenated carbon coatings, it can be assumed that the carbon phase plays a role on the tribological response. In the case of the uncoated ball, the response appears to be governed by the carbon-based material. When both sliding partners are coated, the coefficient of friction in a vacuum is initially quite low indicating that the response is mainly governed by the WS_2 phase. Friction spikes during the remaining time of the test can again be a result of the influence of the carbon phase. The Raman analysis performed on the disk track showed carbon peaks with similar intensity as the ones observed in the as deposited state. Small vestiges related to WS_2 can also be observed. The optical micrograph of the coated ball showed complete wear of the coating. The Raman spectra revealed a significant presence of carbon in combination with WS_2 and WO_3 phases. The compounds identified can be directly related to the tribological response during the test. The periods of low friction can be attributed to the presence of WS_2 in the sliding interface, while the frictional spikes are due to periodic interaction between the carbon phases present on both surfaces in contact.

However, it is still not clear why there is a discrepancy in the tribological response in a vacuum compared to a dry nitrogen environment. Colas et al. [17], also observed a discrepancy in the tribological response of a Ti-doped MoS_2 coating during testing in a vacuum, and under dry N_2 environment; in the latter test, much better performance was achieved. The authors associated the good response in dry N_2 with adsorption of N_2, and, the subsequent occupation of all the

oxidation sites preventing the adsorption of H_2O on the coating. Anomalous wear behavior of MoS_2 coatings in vacuum was also observed by Gardos [52]. In that study, the author also associated the better tribological response in dry N_2, compared to vacuum, to the adsorption of N_2 on the oxidation sites of the MoS_2 and, thus, preventing the adsorption of other species (e.g H_2O) in the MoS_2 films. Considering the vacuum pressures at which Gardos performed the tests were quite similar to the ones used in our study, it is likely that the mechanism proposed by Gardos is herein valid. To better understand these mechanisms, further experiments and simulations are needed. W-S-C coatings with better S/W ratio and varied carbon content will be further investigated at different levels of vacuum, against different counterbodies and under different atmospheres, with the aim of better understanding the tribological behavior of the W-S-C coatings.

4. Conclusions and future work

W-S-C self-lubricating coatings were deposited by close field unbalanced magnetron sputtering in a semi-industrial unit with various power to targets and three target-to-substrate (TSD) distances. The chemical composition, microstructure and mechanical properties were studied as a function of the selected deposition parameters. Tribological studies were performed on a single coating in various testing environments. The main conclusions are:

- TSD has a significant effect on the composition of the coatings, with the longer distances resulting in a higher S/W ratio and the higher overall amount of sulfur. The effect was a result of different scattering behavior of the sputtered species and different level of the bombardment of the growing film with energetic particles.
- The composition of the coatings influenced the microstructure and mechanical properties. Lower S/W ratios and higher C contents resulted in denser microstructures

and increased hardness. X-ray diffraction experiments showed X-ray amorphous structures

- The tribological testing of the selected coatings showed good tribological response while testing in normal air with different loads and at elevated temperatures up to 400 °C. The frictional response was governed by graphitic tribofilms during testing at RT, with low loads. Increasing the loads and/or the testing temperature resulted in the accelerated formation of WS_2 rich tribofilms with a subsequent reduction in friction.
- Testing in a vacuum with steel counterbodies resulted in very high friction, which was due to severe adhesion that led to preferential wear and material transfer from the steel counterbody to the coated disk. Tribological testing in a vacuum with both counterbodies being coated resulted in significant improvement of the tribological response, but instabilities were observed.
- Testing in dry N_2 with both triboelements being coated was optimal with low coefficient of friction and low wear.

The coating that was tribologically tested might not be an ideal solution for providing friction and wear reduction in diverse testing environments since the tribological response in vacuum was unstable. To better understand the relationship between the chemical composition and the tribological response, further studies will be performed on a set of coatings with a higher S/W ratio.

Acknowledgments:

This project has received funding from the European Union's Horizon 2020 research and innovation programme under grant agreement No. 721642: SOLUTION.

The authors would also like to acknowledge the financial support from the projects: ATRITO-0 [co-financed via FEDER (PT2020) POCI-01-0145-FEDER-030446 and FCT (PIDDAC)], On-SURF [co-financed via FEDER (PT2020) POCI-01-0247-FEDER-024521] and CEMMPRE – UID/EMS/00285/2020 [co-financed via FEDER and FCT (COMPETE)]

T.P. acknowledges support from the project Novel nanostructures for engineering applications No. CZ.02.1.01/0.0/0.0/16_026/0008396 and CAAS No. CZ.02.1.01/0.0/0.0/16_019/0000778

List of references:

[1] Spalvins T. Lubrication with Sputtered MoS $_2$ Films. A S L E Trans 1971;14:267–74. doi:10.1080/05698197108983252.

[2] Prasad S, Zabinski J. Super slippery solids. Nature 1997;387:761. doi:10.1038/42820.

[3] Scharf TW, Rajendran A, Banerjee R, Sequeda F. Growth, structure and friction behavior of titanium doped tungsten disulphide (Ti-WS2) nanocomposite thin films. Thin Solid Films 2009;517:5666–75. doi:https://doi.org/10.1016/j.tsf.2009.02.103.

[4] Xu S, Sun J, Weng L, Hua Y, Liu W, Neville A, et al. In-situ friction and wear responses of WS2 films to space environment: Vacuum and atomic oxygen. Appl Surf Sci 2018;447:368–73. doi:10.1016/J.APSUSC.2018.04.012.

[5] Xu S, Hu M, Sun J, Weng L, Liu W, Gao X. A simple strategy to tailor the microstructure

and wear-resistance of sputtered WS2 films. Mater Lett 2018;216:179–81. doi:10.1016/J.MATLET.2018.01.027.

[6] Polcar T, Cavaleiro A. Review on self-lubricant transition metal dichalcogenide nanocomposite coatings alloyed with carbon. Surf Coatings Technol 2011;206:686–95. doi:10.1016/J.SURFCOAT.2011.03.004.

[7] Nossa A, Cavaleiro A. The influence of the addition of C and N on the wear behaviour of W–S–C/N coatings. Surf Coatings Technol 2001;142–144:984–91. doi:10.1016/S0257-8972(01)01249-X.

[8] Spalvins T. Lubrication With Sputtered MoS2 Films: Principles, Operation, Limitations. NASA Tech Memo 105292 1991.

[9] Teer DG, Hampshire J, Fox V, Bellido-Gonzalez V. The tribological properties of MoS2/metal composite coatings deposited by closed field magnetron sputtering. Surf Coatings Technol 1997;94–95:572–7. doi:https://doi.org/10.1016/S0257-8972(97)00498-2.

[10] Voevodin AA, O'Neill JP, Zabinski JS. Nanocomposite tribological coatings for aerospace applications. Surf Coatings Technol 1999;116–119:36–45. doi:10.1016/S0257-8972(99)00228-5.

[11] Polcar T, Cavaleiro A. Self-adaptive low friction coatings based on transition metal dichalcogenides. Thin Solid Films 2011;519:4037–44. doi:10.1016/J.TSF.2011.01.180.

[12] Nossa A, Cavaleiro A, Carvalho NJM, Kooi BJ, De Hosson JTM. On the microstructure of tungsten disulfide films alloyed with carbon and nitrogen. Thin Solid Films

2005;484:389–95. doi:10.1016/J.TSF.2005.02.018.

[13] Polcar T, Evaristo M, Stueber M, Cavaleiro A. Mechanical and tribological properties of sputtered Mo-Se-C coatings. Wear 2009;266:393–7. doi:10.1016/j.wear.2008.04.010.

[14] Nossa A, Cavaleiro A. Chemical and physical characterization of C(N)-doped W–S sputtered films. J Mater Res 2004;19:2356–65. doi:10.1557/JMR.2004.0293.

[15] Fox VC, Renevier N, Teer DG, Hampshire J, Rigato V. The structure of tribologically improved MoS2–metal composite coatings and their industrial applications. Surf Coatings Technol 1999;116–119:492–7. doi:https://doi.org/10.1016/S0257-8972(99)00193-0.

[16] Teer DG. New solid lubricant coatings. Wear 2001;251:1068–74. doi:10.1016/S0043-1648(01)00764-5.

[17] Colas G, Saulot A, Bouscharain N, Godeau C, Michel Y, Berthier Y. How far does contamination help dry lubrication efficiency? Tribol Int 2013;65:177–89. doi:10.1016/J.TRIBOINT.2012.12.011.

[18] Evaristo M, Polcar T, Cavaleiro A. Can {W-Se-C} Coatings Be Competitive to {W-S-C} Ones? Plasma Process Polym 2009;6:S92--S95.

[19] Domínguez-Meister S, Conte M, Igartua A, Rojas TC, Sánchez-López JC. Self-Lubricity of WSe_x Nanocomposite Coatings. ACS Appl Mater Interfaces 2015;7:7979–86. doi:10.1021/am508939s.

[20] Dominguez-Meister S, Justo A, Sanchez-Lopez JC. Synthesis and tribological properties of WSex films prepared by magnetron sputtering. Mater Chem Phys 2013;142:186–94.

doi:10.1016/J.MATCHEMPHYS.2013.07.004.

[21] Cao H, De Hosson JTM, Pei Y. Effect of carbon concentration and argon flow rate on the microstructure and triboperformance of magnetron sputtered WS2/a-C coatings. Surf Coatings Technol 2017;332:142–52. doi:10.1016/J.SURFCOAT.2017.06.087.

[22] Cao H, Wen F, Kumar S, Rudolf P, De Hosson JTM, Pei Y. On the S/W stoichiometry and triboperformance of WSxC(H) coatings deposited by magnetron sputtering. Surf Coatings Technol 2018. doi:10.1016/J.SURFCOAT.2018.04.040.

[23] Oliver WC, Pharr GM. An improved technique for determining hardness and elastic modulus using load and displacement sensing indentation experiments. J Mater Res 1992;7:1564–83. doi:10.1557/JMR.1992.1564.

[24] Polcar T, Evaristo M, Cavaleiro A. Friction of Self-Lubricating W-S-C Sputtered Coatings Sliding Under Increasing Load. Plasma Process Polym 2007;4:S541–6. doi:10.1002/ppap.200731402.

[25] Polcar T, Evaristo M, Cavaleiro A. The tribological behavior of W–S–C films in pin-on-disk testing at elevated temperature. Vacuum 2007;81:1439–42. doi:10.1016/J.VACUUM.2007.04.010.

[26] Petrov I, Barna PB, Hultman L, Greene JE. Microstructural evolution during film growth. J Vac Sci Technol A Vacuum, Surfaces, Film 2003;21:S117–28. doi:10.1116/1.1601610.

[27] Särhammar E, Strandberg E, Sundberg J, Nyberg H, Kubart T, Jacobson S, et al. Mechanisms for compositional variations of coatings sputtered from a WS2 target. Surf Coatings Technol 2014;252:186–90. doi:10.1016/j.surfcoat.2014.04.066.

[28] Rumaner LE, Tazawa T, Ohuchi FS. Compositional change of (0001) WS_2 surfaces induced by ion beam bombardment with energies between 100 and 1500 eV. J Vac Sci Technol A Vacuum, Surfaces, Film 1994;12:2451–6. doi:10.1116/1.579192.

[29] Weise G, Mattern N, Hermann H, Teresiak A, Bächer I, Brückner W, et al. Preparation, structure and properties of MoSx films. Thin Solid Films 1997;298:98–106. doi:https://doi.org/10.1016/S0040-6090(96)09165-1.

[30] Abad MD, Muñoz-Márquez MA, El Mrabet S, Justo A, Sánchez-López JC. Tailored synthesis of nanostructured WC/a-C coatings by dual magnetron sputtering. Surf Coatings Technol 2010;204:3490–500. doi:10.1016/J.SURFCOAT.2010.04.019.

[31] Voevodin AA, O'Neill JP, Prasad S V., Zabinski JS. Nanocrystalline WC and WC/a-C composite coatings produced from intersected plasma fluxes at low deposition temperatures. J Vac Sci Technol A Vacuum, Surfaces, Film 1999;17:986–92. doi:10.1116/1.581674.

[32] Evaristo M, Azevedo R, Palacio C, Cavaleiro A. Influence of the silicon and oxygen content on the properties of non-hydrogenated amorphous carbon coatings. Diam Relat Mater 2016;70:201–10. doi:10.1016/J.DIAMOND.2016.10.024.

[33] Polcar T, Evaristo M, Cavaleiro A. The tribological behavior of W–S–C films in pin-on-disk testing at elevated temperature. Vacuum 2007;81:1439–42. doi:10.1016/J.VACUUM.2007.04.010.

[34] Leyland A, Matthews A. On the significance of the H/E ratio in wear control: a nanocomposite coating approach to optimised tribological behaviour. Wear 2000;246:1–11. doi:10.1016/S0043-1648(00)00488-9.

[35] Musil J, Kunc F, Zeman H, Poláková H. Relationships between hardness, Young's modulus and elastic recovery in hard nanocomposite coatings. Surf Coatings Technol 2002;154:304–13. doi:10.1016/S0257-8972(01)01714-5.

[36] Berkdemir A, Gutiérrez HR, Botello-Méndez AR, Perea-López N, Elías AL, Chia C-I, et al. Identification of individual and few layers of WS2 using Raman Spectroscopy. Sci Rep 2013;3:1755. doi:10.1038/srep01755.

[37] Wahl KJ, Seitzman LE, Bolster RN, Singer IL. Low-friction, high-endurance, ion-beam-deposited PbMoS coatings. Surf Coatings Technol 1995;73:152–9. doi:10.1016/0257-8972(94)02383-2.

[38] Zabinski JS, Donley MS, Dyhouse VJ, McDevitt NT. Chemical and tribological characterization of PbOMoS2 films grown by pulsed laser deposition. Thin Solid Films 1992;214:156–63. doi:10.1016/0040-6090(92)90764-3.

[39] Kohli AK, Prakash B. Contact pressure dependency in frictional behavior of burnished molybdenum disulphide coatings. Tribol Trans 2001;44:147–51. doi:10.1080/10402000108982439.

[40] Singer IL, Bolster RN, Wegand J, Fayeulle S, Stupp BC. Hertzian stress contribution to low friction behavior of thin MoS 2 coatings. Appl Phys Lett 1990;57:995–7. doi:10.1063/1.104276.

[41] Nicolini P, Capozza R, Restuccia P, Polcar T. Structural Ordering of Molybdenum Disulfide Studied via Reactive Molecular Dynamics Simulations. ACS Appl Mater Interfaces 2018;10:8937–46. doi:10.1021/acsami.7b17960.

[42] Voevodin AA, Zabinski JS. Supertough wear-resistant coatings with “chameleon” surface adaptation. Thin Solid Films 2000;370:223–31. doi:10.1016/S0040-6090(00)00917-2.

[43] Krumpiegl T, Meerkamm H, Fruth W, Schaufler C, Erkens G, Böhner H. Amorphous carbon coatings and their tribological behaviour at high temperatures and in high vacuum. Surf. Coatings Technol., vol. 120–121, 1999, p. 555–60. doi:10.1016/S0257-8972(99)00435-1.

[44] Konca E, Cheng YT, Weiner AM, Dasch JM, Alpas AT. Elevated temperature tribological behavior of non-hydrogenated diamond-like carbon coatings against 319 aluminum alloy. Surf Coatings Technol 2006;200:3996–4005. doi:10.1016/j.surfcoat.2005.02.202.

[45] Andersson J, Erck RA, Erdemir A. Friction of diamond-like carbon films in different atmospheres. Wear 2003;254:1070–5. doi:10.1016/S0043-1648(03)00336-3.

[46] Miyoshi K. Considerations in vacuum tribology (adhesion, friction, wear, and solid lubrication in vacuum). Tribol Int 1999;32:605–16. doi:10.1016/S0301-679X(99)00093-6.

[47] Colas G, Saulot A, Regis E, Berthier Y. Investigation of crystalline and amorphous MoS2 based coatings: Towards developing new coatings for space applications. Wear 2015;330–331:448–60. doi:10.1016/j.wear.2015.01.011.

[48] Gustavsson F, Jacobson S, Cavaleiro A, Polcar T. Frictional behavior of self-adaptive nanostructural Mo-Se-C coatings in different sliding conditions. Wear 2013;303:286–96. doi:10.1016/j.wear.2013.03.032.

[49] Sundberg J, Nyberg H, Särhammar E, Gustavsson F, Kubart T, Nyberg T, et al. Influence of Ti addition on the structure and properties of low-friction W–S–C coatings. Surf Coatings Technol 2013;232:340–8. doi:10.1016/J.SURFCOAT.2013.05.032.

[50] Polcar T, Gustavsson F, Thersleff T, Jacobson S, Cavaleiro A. Complex frictional analysis of self-lubricant W-S-C/Cr coating. Faraday Discuss 2012;156:383. doi:10.1039/c2fd00003b.

[51] Kurahashi Y, Tanaka H, Terayama M, Sugimura J. Effects of Environmental Gas and Trace Water on the Friction of DLC Sliding with Metals. Micromachines 2017;8:217. doi:10.3390/mi8070217.

[52] Gardos MN. Anomalous wear behavior of MoS2 films in moderate vacuum and dry nitrogen. Tribol Lett 1995;1:67–85. doi:10.1007/BF00157977.

Supplementary Information

Synthesis, microstructure and mechanical properties of W-S-C self-lubricant thin films deposited by magnetron sputtering

Todor Vuchkov, Manuel Evaristo, Talha bin Yaqub, Tomas Polcar, Albano Cavaleiro

Tribological properties at different RH:

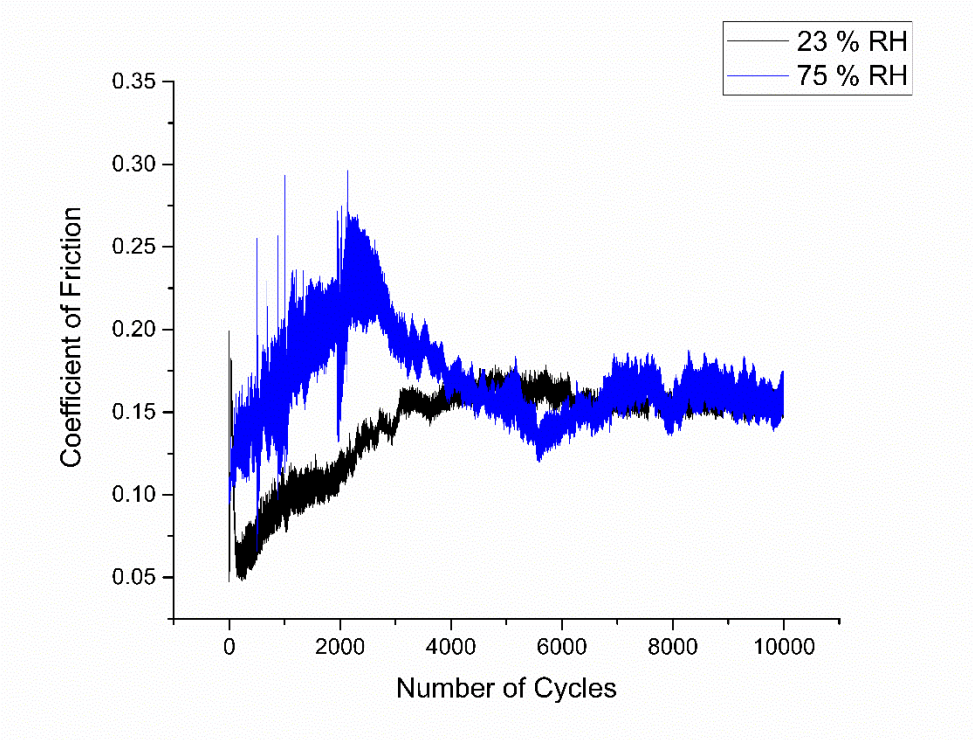

Figure S1 Tribological response at different level of humidity

In order to study the potential effect of the relative humidity RH, tribological tests were performed at two different RH, 23 % and 75 % (15 N of load, 10 mm DIN 100Cr6 ball). The main difference between the friction curves are observed during the running-in period, with the test performed at higher RH showing higher COF. Nevertheless, the frictional response stabilized at values of ~0.15-0.2. Therefore, we do not expect significant difference of the tribological performance in relation to the RH (30-45 %) typically encountered in the laboratory environment.

Tribological response during testing at elevated temperature:

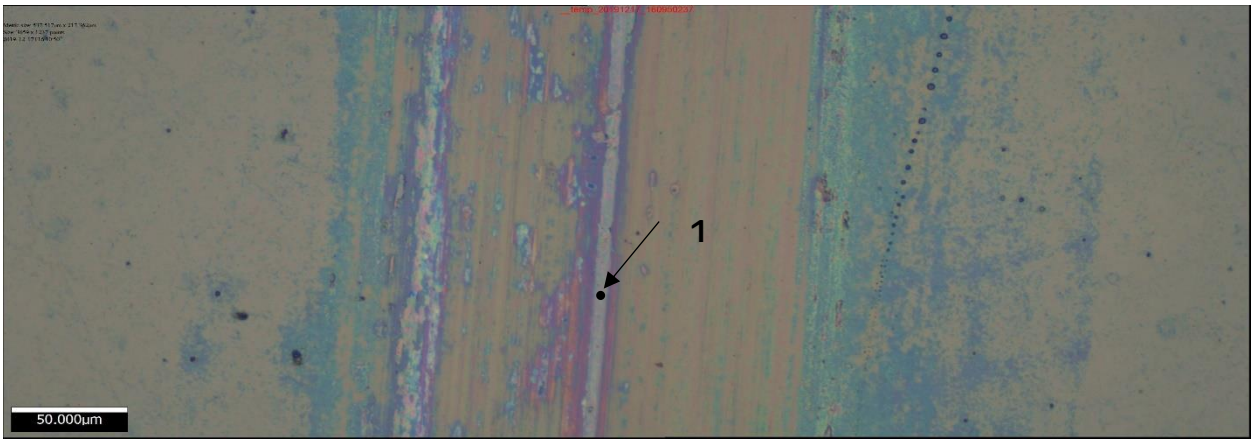

Figure S2 Optical micrograph from the wear track after testing at a temperature of 400°C

a) b)

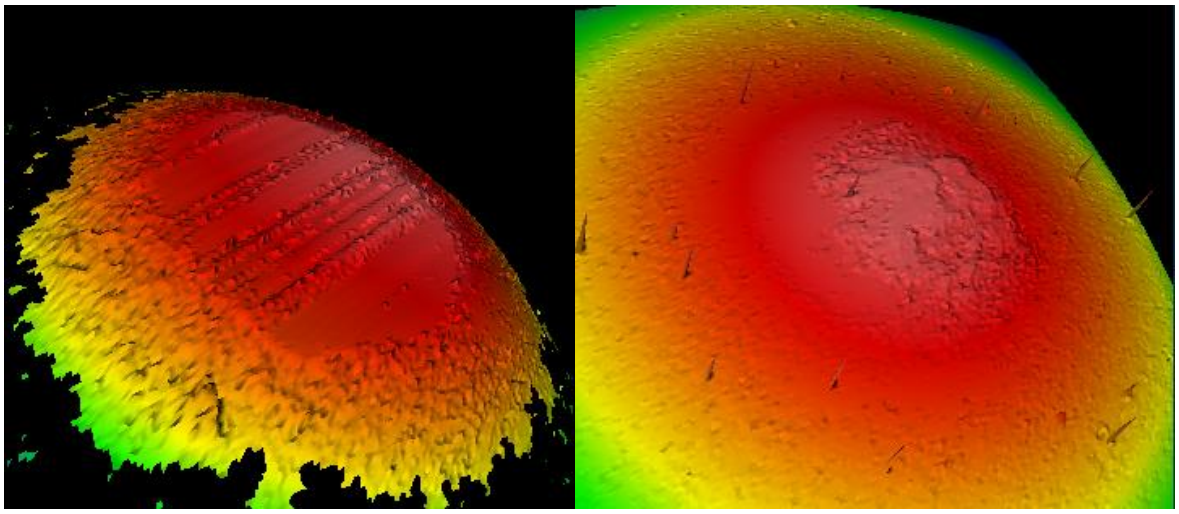

Figure S3 3D topography of the bearing steel balls after a) testing at 100°C and b) testing at 100°C

Figure S2 is an optical micrograph of a typical wear track after testing at an elevated temperature of 200°C. The typical location where the Raman analysis was performed was marked with 1. The 3D topography of the bearing steel balls after testing at 100°C and 300°C are shown in Figure S3 a) and b), respectively. The wear scar is evident after testing at 100°C, unlike the one observed after testing at a temperature of 300°C. An optical micrograph of the bearing steel ball after testing at a temperature of 300°C is shown in Figure S4, showing the patches of transferred material.

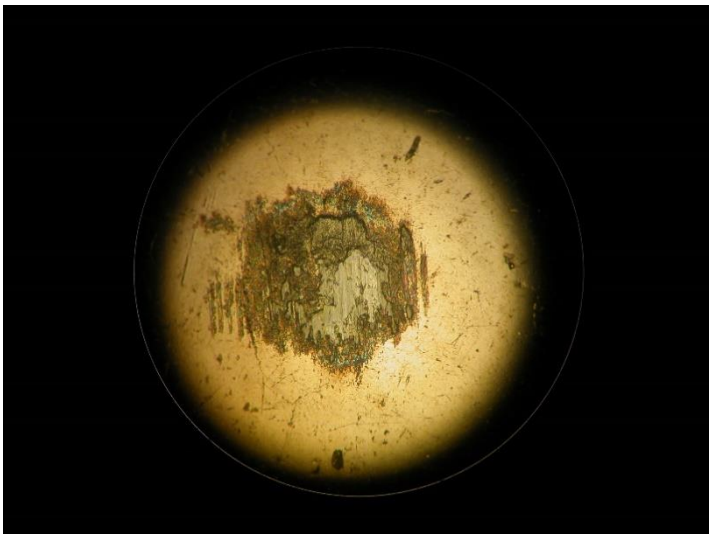

Figure S4 Optical micrograph from the bearing steel ball after testing at 300°C